Elastic Modulus Of Steel Fiber-reinforced Concrete: Application Of Optimized Algorithms

Xi Chen*

School of Civil Engineering, Sifang College of Shijiazhuang Railway University, Shijiazhuang City, Hebei Province, China

Corresponding author. E-mail: chenxi_870209@163.com

Received: Apr. 12, 2025; Accepted: Jul. 13, 2025

Incorporating steel fibers into plain concrete has been shown to effectively improve the load-bearing capacity of structural elements. As of now, the impact of fibers on the fundamental mechanical characteristics of Steel Fiber Reinforced Concrete (SFRC) and the associated uncertainties remain inadequately characterized, and precise models for predicting their mechanical properties are lacking. This significantly restricts the applicability in actual buildings. The study investigates various factors affecting settlement, including the water-tocement ratio, sand-to-cement mass ratio, coarse aggregate-to-cement mass proportion, fiber reinforcement coefficient, fiber morphology parameter, coarse aggregate size, superplasticizer-to-cement mass ratio, and fiber tensile yield strength. This research evaluates three approaches for forecasting E_{cy}, emphasizing the use of a hybrid optimization approach, the Electric Eel Foraging (EEF), with Gradient Boosting regression (GB) and Random Forests regression (RF) methods. Based on the available data, it is likely that RF-EEF and GB-EEF will be able to accurately compute the E_{cy}. The GB-EEF approach exhibited a high level of functional dependability throughout the training and evaluation phases, as shown by the R^2 values of 0.9764 and 0.9822 . Findings of 0.9892 and 0.9965 , achieved utilizing the RF-EEF technique, were relatively close. Feature importance depicted the highest impact of coarse aggregates to cement ratio and fiber kinds on the target by 0.9961 and 0.995.

Keywords: Reinforced concrete; Steel fiber; Machine learning; Electric eel foraging optimizer; Parameter significance

http://dx.doi.org/10.6180/jase.202605_29(5).0020

1. Introduction

In 2020, the annual universal usage of cement-based composite was nearly 14 billion cubic meters, which was about 4.4 tons per individual [1]. On the other hand, the use of cementbased composite also brings issues that restrict its excessive use in civil engineering [2]. For instance, one of these defects is the low tensional resistance of concrete, which is about 1.16 to 1.18 of compacting resistance [3]. Overall, enhanced cement-based composite is still prone to cracking. To solve this issue, scientists proposed a approach that diminishes this issue to some extent by adding steel fibers to concrete. This approach is called steel fiber reinforced concrete (SFRC). The proposed resolution has been very effective in declining the amount of concrete gapping & expanding its resistance [4].

The first study on fiber-enhanced concrete was conducted by Yu et al. [5] in early 1874. He aimed to enhance the tensile strength of concrete by using iron alloy. Upon completion of this study, other research followed, focusing on various aspects of fiber-enhanced concrete performance, including uniaxial and multi-axial mechanical properties [6–8], permanence [9, 10], exhaustion & resistant attributes against catastrophes [11, 12] & micro-structure [13]. Recent mesoscale statistical evaluations [13, 14] have been published to highlight the critical failure mechanisms of steel fiber-enhanced concrete under different external loads. Furthermore, several innovative fiber types have been sug-

gested for enhancement [6], & the application of magnetic fields has been investigated to align the steel fibers during the casting procedure [14]. Similar instigations have shown that there are notable differences between the properties of fiber-enhanced concrete and ordinary concrete. The unique resistance and flexibility of steel fibers provide steel fiber-enhanced concrete with effective bridging capabilities after cracking, as well as enhanced mechanical attributes when subjected to tensile, shear, and torsional loads [5]. A large inconsistency in the materials used is often the primary reason for the variations in mechanical attributes. Steel fibers are capable of significantly inhibiting the propagation of macro-cracks; however, they generally reduce the spread of the novel admixture compared to conventional cement-based composites at the same water-tobinder ratio. This reduction is most likely due to the interaction between the aggregate and the fibers [5]. To forecast the crucial mechanical features of fiber-improved concrete (such as elastic modulus), models need to be developed that can be easily integrated into engineering design codes. However, existing models used by researchers lack sufficient accuracy and sometimes fail to reflect the physical relationships between the model and the characteristics of the predicted properties. Abbass et al. [15], Luo et al. [16], & Jamshidi and Arefi [17] previously proposed simple linear formulas to estimate the mechanical features of steel fiber-enhanced concrete, based on their empirical findings. The consensus among all these studies is that the fiber volume fraction and the water-to-binder ratio are key agents influencing the strength and behavior of steel fiber- enhanced concrete. Wu et al. [18] applied a composite material mixing strategy and found a significant correlation between the strength and deformation properties and the relative elastic modulus of steel fibers in relation to concrete. He subsequently proposed two experimental equations. Zhu [19], suggested equations for calculating the tensile strength, bending strength, and elastic modulus of steel fiber-enhanced concrete, based on correlations between these properties and the compressive strength of steel fiber-enhanced concrete. However, the models used to estimate the compressive strength of steel fiber-enhanced concrete were not included in their study. In general, the prediction of mechanical properties in these models is based on experimental testing, but a comprehensive validation of these models' accuracy is not always provided [20].

Machine learning approaches have been used in recent years as an efficient and innovative method to determine the mechanical properties of engineering problems [21–27]. Açikgenç et al. [28] employed a back-propagation artificial neural network to estimate the compressive strength of steel fiber-enhanced concrete, considering key factors such as maximum aggregate size, fiber volume fraction, and the length and diameter of the fibers. In another research, Awolusi et al. [29] used the compacting resistance & split tensional resistance of 100 mm thick cubes estimated by artificial neural network of fiber enhanced concrete to estimate slump. In the research conducted by Karahan et al. [30], the solidified resistance of fiber-enhanced concrete with various amounts of fly ash was estimated using artificial neural network & multivariate non-linear regression. The models that are based on black box data to evaluate the mechanical features of fiber enhanced concrete have deficiencies, but they are often accurate enough in estimation. These models often lack a clear statement, which restricts their availability, & they intrinsically do not provide sufficient representations of the underlying physical tactic.

This research aims to address the aforementioned difficulties. The primary step involved searching for and screening accessible test data to establish a comprehensive database encompassing the mechanical attributes of $SFRC$ and its mix ratios (mass contents of cement, water, sand, gravel, water reducer, and fiber), coarse aggregate size, fiber characteristics, and any other pertinent information. This study measured the elastic modulus (E_{cy}) of $SFRC$ via several tree-based regression methodologies. The aim of this work was to forecast the E_{cy} by the use of several machine learning approaches derived from tree-based regression methodologies. Random Forests regression (RF) and Gradient Boosting regression (GB) are the names of the tree-based models that were taken into account in the context of this specific inquiry. New studies have shown that the hyperparameters of the RF and GB significantly affect the accuracy and performance of the system. By using metaheuristic optimization techniques, these hyperparameters may be generated as effectively as feasible to achieve the intended outcomes. To help in this quest, a recently developed technique called electric eel foraging (EEF) has been selected. This is primarily due to the fact that too few samples were studied, which prevented the findings from being broadly generalized. For the purpose of the research, the elastic modulus of concrete was determined 113 times overall using information from various sources. These sets then went through two rounds of different learning and assessment processes. For a more detailed explanation, 75% of the dataset was used as a training dataset and 25% as an evaluation subset throughout the development and testing of the proposed framework. The steel fiber-reinforced concrete's elastic modulus, which is a property of concrete, is calculated using eight different agents.

2. Methods

2.1. Dataset description

The combination of steel fibers in plain concrete effectively improves the bearing capacity of structural elements. The influence of fibers on the fundamental mechanical properties of steel fiber-reinforced concrete, such as its modulus of elasticity (E_{cy}) requires accurate information that is essential for prediction methods using artificial intelligence approaches. Therefore, in order to make relevant predictions, a series of data from valid technical literature is needed to perform the forecasting operation. In this article, 113 data points have been collected from reliable articles in the technical literature [31–41]. The data is divided into two sets: a training set, which includes 75% of the data, and a testing set, which includes 25% of the total data, in order to ensure accurate estimation. Also, the correct selection of input variables to perform operations on them is one of the key standards in doing it correctly & accurately. To further evaluate the robustness of the proposed model, a 4-fold cross-validation (CV) procedure was conducted. The dataset was divided into four equal subsets, where each subset was used once as a test set while the remaining three were used for training. The process was repeated four times, and the average results were computed. The performance metrics across all folds are summarized in Table 1. These results demonstrate consistent model performance across different splits of the data, confirming the model's stability and generalization capability.

In Table 2, using a series of commonly used & well-known evaluation indices including min, max, skewness, standard deviation, variation, mean & kurtosis. A detailed examination of the characteristics of the agents required for estimation in the abnormal state has been carried out. In this table, the data are examined in two divided parts of training & testing. It also shows that the prediction includes 9 input agents & one outcome agent, which includes: water-tocement proportion W/C, mass ratio of sand / cement S/C, mass ratio of coarse aggregates / cement CA/C, fiber enhancement coefficient $R = \left(V_f \times L_f/D_f\right)$, fiber shape variable ρ_f, size of coarse aggregate $S_{\max}$, mass proportion of superplasticizer / cement SP/C, fiber tensional yield resistance f_f& fiber kinds including: Hooked (coded as 1), Mill-cut (coded as 2) and Crimped (coded as 3). The result variable means elastic modulus of steel fiber enhanced concrete E_{cy}. These evaluation indices provide important attributes of the parameters in the two mentioned fields and effectively help scholars & studiers in correctly understanding the data, such as how they are distributed and the common points of their properties.

Next, for a better understanding of the data, another type of visualization is used to examine the characteristics of the variables more accurately and easily. For instance, the diagram presented in Fig. 1 is known as the Pearson correlation chart. It is a statistical tool used to evaluate the linear link between two factors. This analysis can significantly influence the development of robust artificial intelligence methodologies. The correlation coefficient ranges from -1 to 1 . A value of 1 indicates a perfect positive correlation, meaning that an increase in one parameter corresponds to an increase in the other variable. A value of -1 indicates a perfect negative correlation, meaning that an increase in one parameter results in a decrease in the other. A value of 0 indicates no correlation, meaning that variations in one parameter do not affect changes in the other parameter. The correlation levels can be sorted as follows: a correlation between 0 and 0.1 is considered insignificant, between 0.1 and 0.3 is weak, between 0.3 and 0.5 is moderate, between 0.5 and 0.7 is robust, and between 0.7 and 1.0 is very strong. Positive values indicate a direct correlation, while negative values indicate an inverse correlation. However, there are limitations to this analysis. For instance, this graph only estimates linear links and may not capture more complex relationships. It is also sensitive to outliers, which can have a significant impact on the correlation coefficient. Overall, Pearson's correlation is a valuable tool for understanding the connection between two agents, provided its assumptions are met and the context of the data is considered. In this graph, we can see the connection among 9 input variables against the result agent. The result shows a robust correlation of 0.76 among S/C&W/C agents, while the correlation among SP/C&ρ_t variables is relatively feeble with a number of -0.43 .

Table 1. 4-Fold Cross-Validation Results

Fold	R^2	RMSE	MAE
1	0.999	0.3315	0.1588
2	0.9878	0.3589	0.1788
3	0.9899	0.3555	0.1733
4	0.992	0.345	0.1688
Avg	0.9928	0.3475	0.1697

Also, Fig. 2 shows a linkage chart commonly used in data analysis to visualize the relationships among multiple input parameters and a target parameter. Each colored line corresponds to a specific index in the data, linking the values of the input parameters to the outcome parameter. The different colors in the chart represent various types of data. The size of the lines - whether increasing, decreasing, or remaining fixed - can indicate the relationship between the parameters. For instance, you may observe that cer-

Table 2. Statistical properties of input and target variables

Index	Input variables									Target
	W/C	S/C	CA/C	$S_{\max}$	SP/C	FT	R	ρ_f	f_f	E_{cy}
Unit	-	-	-	mm	-	-	%	-	MPa	GPa
					Training dataset					
Min.	0.3	0.81	1.57	10	0.0	1.0	0.0	0.5	500	23.7
Max.	0.7	3.251	4.764	25	0.04	3.0	175	1.0	2000	45.9
Skew.	1.051	0.423	1.027	-1.514	1.978	2.560	1.223	-2.246	1.289	0.469
St.D.	0.099	0.632	0.713	3.191	0.009	0.555	32.027	0.163	281.31	4.201
Var.	0.010	0.399	0.508	10.185	0.0	0.308	1025.73	0.027	79137.63	17.649
Avg.	0.448	2.013	2.636	18.835	0.007	1.212	42.007	0.935	1156.81	34.545
Kurt.	0.305	-0.719	1.329	2.857	5.234	5.285	2.248	3.245	3.282	0.210
Index	Input variables									Target
	W/C	S/C	CA/C	$S_{\max}$	SP/C	FT	R	ρ_f	f_f	E_{cy}
Unit	-	-	-	mm	-	-	%	-	MPa	GPa
					Testing dataset					
Min.	0.3	0.81	1.57	10	0.0	1.0	0.0	0.5	500	28.9
Max.	0.7	3.105	4.805	22	0.013	3.0	116.66	1.0	2000	46.5
Skew.	0.679	0.174	1.309	-2.640	0.71	2.806	0.961	-2.391	1.130	0.408
St.D.	0.112	0.561	0.788	2.260	0.004	0.467	26.71	0.158	369.62	4.403
Var.	0.012	0.314	0.620	5.106	0.0	0.218	713.72	0.025	136621.17	19.384
Avg.	0.443	2.079	2.629	19.036	0.005	1.179	40.01	0.938	1196.4	35.925
Kurt.	-0.538	-0.470	1.857	8.783	-0.496	7.846	0.715	4.243	1.228	-0.559

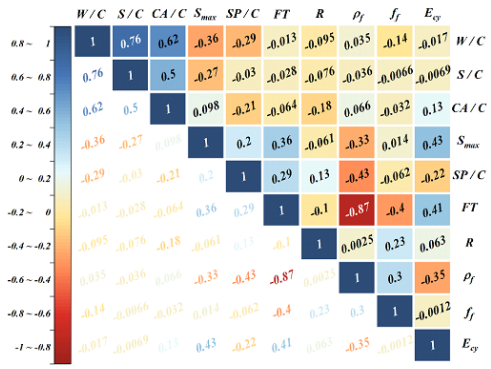

Fig. 1. Correlation type of statistics: Pearson

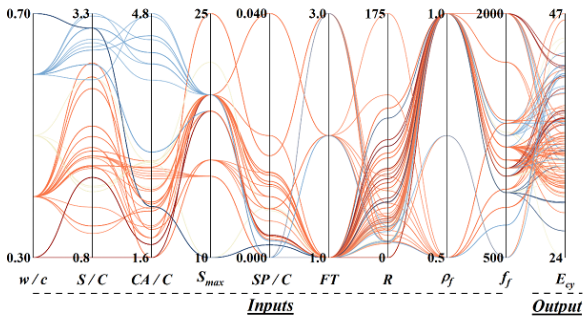

Fig. 2. Linked line of input and target variables

tain inputs result in higher or lower values in the outcome agent. Lines that move together may suggest correlations between specific input parameters and the outcome parameter. The expansion or contraction of the lines can demonstrate the variability of the outcome based on different input combinations. Additionally, the FT parameter in the chart consists of three sections. The first section corresponds to Hooked fibers, the second to Mill-cut fibers, and the third to Crimped fibers. In summary, line graphs are an effective way to visualize complex relationships within data, enabling analysts to extract insights from multiple parameters simultaneously. They are especially valuable in fields like engineering, and in any area where understanding the relationship between inputs and outcomes is critical.

The assessment of Table. 3indicates that the model's input agents are arranged according to their significance in predicting the modulus of elasticity of steel fiber reinforced concrete (E_{cy}).

The S_1 values serve as an index of the relative significance of each parameter; the closer this value is to 1 , the bigger the parameter's influence on the model output. The assessment indicated that the agents (CA/C and $S_{\max}$) and (FT and f_f) are the most significant factors, whereas the variables (SP/C) and (R) are equally critical but ranked lower than the former group. Ultimately, proportions such as W/C and S/C, contrary to assumptions, exert a declined influence relative to other parameters. This may indicate the model's superior effectiveness in assessing microstruc-

tural effects compared to macroscopic effects.

Table 3. feature importance analysis by FAST methodology

Parameter	S1 value from highest to smallest
CA/C	0.9961
FT	0.995
$S_{\max}$	0.9807
f_f	0.9676
SP/C	0.9368
R	0.8099
ρ_f	0.701
W/C	0.6472
S/C	0.4698

2.2. Adjuster optimization: Electric eel foraging (EEF)

Electric Eel Foraging Optimization begins by adjusting control variables, such as the maximum repetition count and the size of the electric eel population. A group of eels is randomly initialized, and each eel exhibits interactive behavior to explore resources when its energy level (E) exceeds 1. When at rest, moving, or chasing, each eel exploits resources with equal probability if its energy level (E) is at or below 1. Candidate solutions are generated and evaluated against current options, with the most effective solution being refined through iterative updates. As the iterations progress, the energy level (E) decreases, causing a shift from exploration to exploitation. The interactive process continues until a predefined stopping criterion is met, at which point the best solution is recorded.

Electric eel foraging optimization has shown exceptional function in discovery, regional improved avoidance, and utilization when subjected to thorough testing, outperforming other enhancement methods. Its adaptability encompasses a wide range of enhancement challenges, including those characterized by multiple constraints and parameters. Importantly, electric eel foraging optimization takes into account the ethical sizes of issue-solving. Eels possess the ability to detect the situation of their prey through low-level electrical emissions, allowing them to set up their situations actively. During searching, when an eel detects the presence of prey, it shifts to a possible situation; if no prey is sensed, it stays in its present situation [42, 43].

$$X_i(t+1) = \begin{cases} X_i(t) & \text{fit } (X_i(t) \le (\vartheta_i(t+1))) \\ \vartheta_i(t+1) & \text{fit } (X_i(t) > (\vartheta_i(t+1))) \end{cases} \quad (1)$$

The term fit $(X_i(t))$ donates the fitness associated with the applicant situation of the ith electric eel. Here, X_i represented the place of an eel that has been accidentally selected from the existing group, while ϑ_i indicates the situation of an accidentally chosen power supply resource. Electric eel foraging optimization setting up requires the explanation of control variables, including the highest repetition count & the crowd size of the electric eels. A collection of eels is manufactured with an accidental broadcast. In each repetition, when the energy standard E exceeds 1, each eel participates in discovery through its inter-active acting. When the energy standard E is at or below 1, every eel has an equal chance of participating in activities such as relaxing, moving, or chasing. To manufacture novel candidate solution, each case is evaluated against every eel, and these resolutions are then compared to the existing ones. The improved resolution is consistently refined during each level of the repetition strategy. As the repetition advances, the energy standard E declines, leading each eel to shift from discovery to utilization. This inter-active strategy persists until the explained stopping criterion is satisfied. At that moment, the improved resolution obtained thus far is recorded. The operational sequence of the Electric Eel foraging optimization is illustrated in Algorithm 1.

Algorithm 1. The operational sequence of the Electric Eel foraging optimization [42, 43]

```
Create a preliminary value for both N and T
Manufacture a group X_i (i = 1,...,N) at random and estimate the fitness Fit_i
Designate X_b as the improved representation of the eel
while Terminal conditions have not been satisfied do
    for each X_i, where i ranges from 1 to N do
        Revise E values
        if E > 1 then
            Revise the inter-action variables
            Calculate the fitness Fit_i
        else
            if rand > 1/3 then
                Recognize the rest position
                Implement the relaxing attributes
                Assess the fitness Fit_i
            else if rand > 2/3 then
                Implement the transforming attributes
            else
                Recognize the chasing place
                Implement the chasing attributes
        Revise the value of eel
    Upgrade X_b
return the value of X_b
```

2.3. Estimator 1: Random Forests regression (RF)

The Random Forest (RF) method is a leading technique for both regression and classification within decision tree

learning. It demonstrates high efficiency and offers superior regression accuracy compared to other regression methods. The RF model was introduced by L. Breiman in 1986. This model constructs a large number of uncorrelated decision trees during the training process. The model's output is derived by averaging the results from all the individual decision trees. In the RF technique, the learner uses the bootstrap method to train each tree. This procedure involves repeatedly selecting bootstrap specimens from the training dataset and fitting decision trees based on the Gini impurity calculated from these samples. The predicted values for unseen data points are obtained by averaging the prediction results from all regression trees after the training strategy:

$$y = \frac{1}{B}\sum_{b=1}^{B} t_b(x) \tag{2}$$

In the above formula, B represents the number of decision nodes in the decision tree, $t_b(x)$ represents the decision tree prediction number b for input sample x.

The *RF* approach improves forecasting precision by utilizing multiple trees rather than relying on a single tree [44]. This method yields an unbiased ranking of parameters that surpasses the precision of outcomes obtained from CART.

The RF technique finds application in a range of categorization and regression duties, including the forecasting of urban NO2 exposure levels in Japan [45], investigations of landslide vulnerability in China [46], and the mapping of ground-water possible for forecasting crop yields in Iran [47, 48].

2.4. Estimator 2: Gradient Boosting regression (GB)

The Gradient Boosting Regressor (GBR) is a group model that consists of a collection of tree models organized in sequence, where each following model is trained to true, the faults made by the prior one. This machine learning model utilizes enhancing tactics to improve a group of feeble estimative methods, typically decision trees, resulting in a stronger overall model [49]. A gradient enhancing regressor comprising M trees can be expressed as bellows:

$$f_M\left(x_j\right) = \sum_{m}^{M} \gamma_m h_m\left(x_j\right) \tag{3}$$

In this context, h_m represents a feeble learner that exhibits subpar function on its own, while γ_m serves as a scaling standard that improves the contribution of a tree to the overall model. Gradient boosting regressor employs the gradient descent loss subordinate to decline faults by refining the primary forecasting based on the updated prediction. An ultimate model is developed by integrating all preliminary estimates with suitable weights. The GBR model utilized in this investigation is derived from the GBR method available in Scikit - learn.

In gradient boosting, the method is trained by minimizing the loss through repetitive upgrades.

Feeble Learners: In gradient boosting, member models are known as feeble learners because they perform slightly better than accidental guessing.

Loss subordinate: The choice of loss subordinate is very crucial & can vary depending on the normal of the regression issue (eg, mean squared error for continuous aims).

Setting up: Start with a primary forecasting (eg, the mean of the goal quantities).

Iterative training: For each repetition, compute the residuals from the present forecasting.

Fit a feeble learner to these residuals. Update forecasting by adding feeble learner forecasting, scaling the learning rate. Ultimate method: The ultimate method is the sum of all the feeble forecasting of the learners.

Benefits: High precision: often provides high estimative precision.

Adaptability: It can improve various loss subordinates & handle several kinds of data.

2.5. Coupled Estimators: *RF*-*EEF*, and *GB*-*EEF*

A consistent and adaptable *ML* technique which can deal with both regression and classification problems with unexpected durability and precision has been attempted, using *RF* and *GB* models. Improving feature relevance, scalability, and flexibility are further aims of these models. The hyperparameters of the *RF* and *GB* frameworks that substantially impact efficacy may be adjusted by trial and error or optimization. These models attempt to enhance accuracy in prediction and cope with missing data (Table 4).

Optimizing a *RF* model requires fine-tuning critical hyperparameters such as *n_estimators*, *max_depth*, and*max_features*, in addition to hyperparameters for *GB* such as *n_estimators*, *learning_rate*, *max_depth*, *min_samples_split*, and*max_features*, in order to strike a balance between the model's complexity and generalizability. The process is streamlined by initially dividing the dataset into 75% for training and 25% for evaluation. Advanced optimization techniques, such as *EEF*, are then employed to explore different hyperparameter combinations and reduce the RMSE on the validation set. The optimal set of hyperparameters is selected after extensive training and evaluation of several models, considering the distinct effectiveness of every model.

Table 4. The tunned parameters of coupled estimators

$RF-EEF$		$GB-EEF$	
Parameters	Value	Parameters	Value
Maximum number of iterations	200	Maximum number of iterations	200
Number of tries	5	Number of tries	5
Size of population	30	Size of population	20
Other control parameters	-	Other control parameters	-
n_estimators	68	*n_estimators*	75
max_depth	28	*learning_rate*	0.08
min_samples_split	12	*max_depth*	15
max_features	6	*min_samples_split*	20
		max_features	8

2.6. Metrics

A variety of performance criteria, each offering a unique viewpoint on the accuracy and reliability of the model, can be utilized to evaluate the *RF* and *GB* algorithms.

Coefficient of Determination:

$$R^2 = \left(\frac{\sum_{i=1}^{n} (X_i - \bar{X})(S_i - \bar{S})}{\sqrt{\left[\sum_{i=1}^{n} (X_i - X)^2\right]\left[\sum_{i=1}^{n} (S_i - \bar{S})^2\right]}} \right) \quad (4)$$

Root Mean Square Error:

$$RMSE = \sqrt{\frac{1}{n}\sum_{i=1}^{n} (S_i - X_i)^2} \quad (5)$$

Scatter index:

$$SI = \frac{\sqrt{\left(\frac{1}{n}\right)\sum_{i=1}^{n} ((X_i - \bar{X}) - (S_i - \bar{S}))^2}}{\left(\frac{1}{n}\right)\sum_{n=1}^{i} S_i} \quad (6)$$

Normalized Root Mean Square Error:

$$NRMSE = \frac{RMSE}{\bar{S}} \quad (7)$$

Uncertainty with a 95-coincidence level:

$$Un_{95} = 1.96\sqrt{(SD^2 + RMSE^2)} \quad (8)$$

Mean Absolute Error:

$$MAE = \frac{1}{n}\sum_{i=1}^{n} |S_i - X_i| \quad (9)$$

Symmetric Mean Absolute Percentage Error:

$$SMAPE = \frac{1}{n}\sum_{i=1}^{n} \frac{|X_i - S_i|}{\frac{(|X_i| + |S_i|)}{2}} \times 100 \quad (10)$$

Mean Absolute Scaled Error:

$$\text{MASE} = \frac{\frac{1}{n}\sum_{i=1}^{n} |X_i - S_i|}{\frac{1}{n-1}\sum_{i=1}^{n} |X_i - X_{i-1}|} \quad (11)$$

Adjusted R^2 :

$$\text{Adj}_{R^2} = 1 - \frac{(1 - R^2) \times (n-1)}{n - k - 1} \quad (12)$$

The variables X_i, $\bar{X}$, S_i, and $\bar{S}$ indicate the observed E_{cy}, the average of the observed E_{cy}, the anticipated E_{cy}, and the average of the anticipated E_{cy}, respectively, in these calculations. The dataset's row count is represented by n, whereas k is the number of independent variables, or predictors, in the model excluding the intercept.

3. Results and discussion

E_{cy} of steel fiber-reinforced concrete might be easily found by combining the *RF* and *GB* methods with the *EEF* process (commonly called $RF-EEF$ and $GB-EEF$). Figure 3 shows the values of E_{cy} which were measured and anticipated using the $RF-EEF$ and $GB-EEF$ approaches. These were the data that were collected during the investigation's learning and evaluation stages. This figure also shows the proportion of error between the expected and actual E_{cy}. Table. 5 displays the results of the evaluations of the designs acquired at the different learning levels and the evaluations of the process of product creation. Each research model received a score for each statistic at each phase of the study. This was done in an attempt to improve the accuracy of the combined models.

Based on the available data, it is likely that both $RF-EEF$ and $GB-EEF$ will be able to accurately compute the E_{cy}. The $GB-EEF$ approach exhibited a high level of functional dependability throughout the training and evaluation phases of the operation, as shown by the R^2 values of 0.9764 and 0.9822 . Findings of 0.9892 and 0.9965 , achieved utilizing the $RF-EEF$ technique, were relatively close. The findings show that the $RF-EEF$ method functioned superior than the $GB-EEF$ approach regarding R^2 values. The best-performing model was paired with Adj_R^2, and the outcomes revealed a performance pattern resembling one of the an-

ticipated metrics. Merely relying on this figure to assess the model's dependence is insufficient. In order to accomplish this, a thorough analysis of many metrics-including $RMSE, SI, U_{95}, NRMSE, MAE, SMAPE$, and $MASE$-is required. In light of these attributes, a lower score denotes an even greater level of perfect consistency, while a bigger number denotes the reverse. A detailed examination of the numbers related to these aspects shows that the $RF-EEF$ method produces the best accurate results with the least amount of data needed. The $RMSE$ index values produced by the $RF-EEF$ were lowest during the learning and assessment periods, at 0.4376 and 0.2575 , correspondingly. In contrast to the other values achieved, the $GB-EEF$'s training and assessment phases yielded values of 0.6504 and 0.5903 , respectively, indicating a lower degree of dependability.

A comparison between the performance of EEF-based models is made in the Table 5 based on valid indicators. The research shows that U_{95}, representing the 95% confidence level uncertainty measurement, signifies that the exact value will reside within the anticipated and measured range. U_{95} is utilized to evaluate uncertainty, encompassing prediction accuracy and measurement variability. Clear reliance facilitates decision-making. The U_{95} index values for the assessment and training periods were 1.2167 and 0.72 , accordingly, according to the RF_EEF. The comparable U_{95} values for the $GB-EEF$ were 1.8031 and 1.6492. These specifications remained the same throughout the project. Considering assessment variables, logical inference, and rating level, it has been determined that all models are considered reliable and trustworthy. The RF_EEF model is marginally better than the other model in terms of its objective.

The Electric Eel Foraging Optimization (EEF) algorithm was chosen for this investigation due to its demonstrated efficacy in recent benchmark tests involving high-dimensional and nonlinear engineering challenges. While regional enhancer like particle swarm optimization (PSO), genetic algorithm (GA), and Bayesian optimization have been extensively utilized and validated, recent comparative studies indicate that EEF offers improved convergence speed, robustness in evading regional ideal, and an effective balance among utilization and discovery, particularly in intricate optimization scenarios such as ML hyperparameter tuning. Moreover, we sought to explore the application of contemporary metaheuristic methods like EEF within the realm of civil engineering materials modeling, where optimization performance can profoundly influence estimation precision.

Differences % plots in tree and regression systems at each training and testing phase provide a way to assess how much of the variability seen in Fig. 3a may be responsible for the model's incorrect predictions. These charts are produced by deducting the expected values from the actual values to get the error, then estimating the variability of these errors across data points or epochs. Plots that are specific to the training and testing phases are created, showing how the variance percentage changes over time or across samples. Great variability during training but low variance during testing indicates the presence of overfitting, while low variance percentages indicate a high degree of stability and consistency in predictions. These graphs provide important insights into the stability and generalizability of the concept. The distribution results unequivocally show that across all stages, the $RF-EEF$ has continuously surpassed the $GB-EEF$.

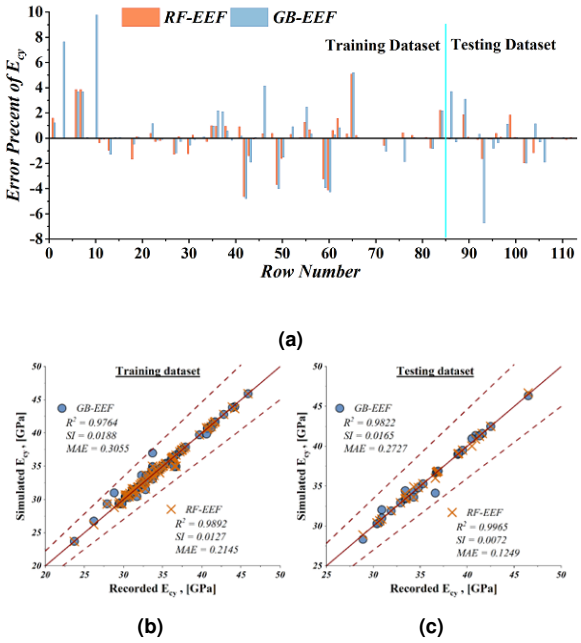

Fig. 3. a) Error distribution between EEF-based models, b) Correlation of simulated and recorded E_{cy} for EEF-based models

The work had to deal with some limited restrictions, such as a roughly small dataset size that makes it hard to use the results in other situations and the lack of fiber distribution variation, which could have changed $SFRC$ features. Also, focusing on short-term mechanical properties like elastic modulus ignores long-term performance issues like creep and shrinking.

Furthermore, the models simplified the complicated behavior of SFRC by leaving out things like fiber-matrix binding and fracture formation. More data needs to be added,

Table 5. performance compartions between EEF-based models

Metrics (Best value)	Coupled estimators				Metrics	Score (High is good)	
	$RF-EEF$	$GB-EEF$	$RF-BWO$	$GB-BWO$		$RF-EEF$	$GB-EEF$
Training dataset							
$R^2(1.0)$	0.9892	0.9764	0.9694	0.9568	R^2	2	1
$RMSE$ (0.0)	0.4376	0.6504	0.4546	0.6757	$RMSE$	2	1
SI (0.0)	0.0127	0.0188	0.0131	0.0195	SI	2	1
$U_{95}(0.0)$	1.2167	1.8031	1.264	1.8732	U_{95}	2	1
$NRMSE$ (0.0)	0.0197	0.0293	0.0204	0.0304	$NRMSE$	2	1
MAE (0.0)	0.2145	0.3055	0.2228	0.3174	MAE	2	1
$SMAPE$ (0.0)	0.6465	0.9233	0.6716	0.9592	$SMAPE$	2	1
$MASE$ (0.0)	0.0443	0.063	0.0460	0.06545	$MASE$	2	1
$Adjusted\_R^2$ (1.0)	0.989	0.9757	0.9593	0.94643	$Adjusted\_R^2$	2	1
Testing dataset							
$R^2(1.0)$	0.9965	0.9822	0.9766	0.9626	R^2	2	1
$RMSE$ (0.0)	0.2575	0.5903	0.2675	0.6133	$RMSE$	2	1
SI (0.0)	0.0072	0.0165	0.0075	0.0171	SI	2	1
$U_{95}(0.0)$	0.72	1.6492	0.7480	1.7134	U_{95}	2	1
$NRMSE$ (0.0)	0.0146	0.0335	0.0152	0.0348	$NRMSE$	2	1
MAE (0.0)	0.1249	0.2727	0.1298	0.2833	MAE	2	1
$SMAPE$ (0.0)	0.3493	0.7972	0.3629	0.8282	$SMAPE$	2	1
$MASE$ (0.0)	0.0246	0.0537	0.0256	0.0558	$MASE$	2	1
$Adjusted\_R^2$ (1.0)	0.9964	0.9811	0.9665	0.9517	$Adjusted\_R^2$	2	1
OBJ	0.2941	0 .4717					

more advanced methods need to be used to study fiber dispersion, and long-term properties need to be checked out in a range of situations. If more aspects were taken into consideration, such as the curing conditions and the strength of the fiber joining, then the predictions would be more accurate. For the purpose of ensuring that full-scale $SFRC$ structures are effective in real-world settings, it is advised that these structures be evaluated personally. Through the production of fundamental tools based on these models, $SFRC$ would be able to continuously increase its appeal within the construction sector.

4. Conclusions

The aim of this research is to create and evaluate the most efficient machine learning, tree, and regression algorithms for estimating the elastic modulus (E_{cy}) of steel fiber reinforced concrete ($SFRC$). A crucial component of the method used to attain this goal was the application of Random Forests regression (RF) and Gradient Boosting regression (GB) software tools. This research utilized a metaheuristic optimization method known as Electric Eel Foraging (EEF).

The FAST sensitivity analysis results indicated that the model input elements were prioritized based on their impact on predicting the modulus of elasticity of steel fiber reinforced concrete (E_{CY}). The parameters CA/C, $S_{\max}$, FT, and f_f exerted the most significant influence, but W/C and S/C had a diminished impact, contrary to expectations, suggesting a more effective emphasis of the model on microstructural effects.

It is likely that both $RF-EEF$ and $GB-EEF$ will be able to accurately compute the E_{cy}. The $GB-EEF$ approach exhibited a high level of functional dependability throughout the training and evaluation phases, as shown by the R^2 values of 0.9764 and 0.9822 . Findings of 0.9892 and 0.9965 , achieved utilizing the $RF-EEF$. The findings show that the $RF-EEF$ functioned superior than the $GB-EEF$ regarding R^2 values. The best-performing model was paired with Adj_R^2, and the outcomes revealed a performance pattern resembling
one of the anticipated metrics.

The U_{95} values for the assessment and training periods were 1.2167 and 0.72 , according to the RF_EEF. The comparable U_{95} for the $GB-EEF$ were 1.8031 and 1.6492. These specifications remained the same throughout the project. Considering assessment variables, logical inference, and rating level, it has been determined that all models are considered reliable and trustworthy. The RF_EEF model is marginally better than the other model in terms of its objective.

The work's disadvantages include a roughly small dataset, absence of fiber dispersion modeling, hyperparameter vulnerability, and focus on short-term attributes without considering creep and shrinkage. For future enhancement, expand the dataset, analyze fiber orientation, evaluate long-term behavior, and investigate different optimization methodologies. Validating models on real struc-

tures and giving easy-to-use tools will help promote *SFRC* in construction.

Acknowledgments

I would like to take this opportunity to acknowledge that there are no individuals or organizations that require acknowledgment for their contributions to this work.

References

[1] B. Bennett, P. Visintin, and T. Xie, (2022) *"Global warming potential of recycled aggregate concrete with supplementary cementitious materials"* **Journal of Building Engineering *52***: 104394. DOI: https://doi.org/10.1016/j.jobe.2022.104394.

[2] R. S. Benemaran, M. Esmaeili-Falak, and M. S. Kordlar, (2024) *"Improvement of recycled aggregate concrete using glass fiber and silica fume"* **Multiscale and Multidisciplinary Modeling, Experiments and Design *7***: 1895–1914. DOI: https://doi.org/10.1007/s41939-023-00313-2.

[3] B. D. G. Sepulveda, P. Visintin, and D. J. Oehlers, (2022) *"Fatigue bond-slip properties of steel reinforcing bars embedded in UHPFRC: Extraction and development of an accumulated damage law"* **Case Studies in Construction Materials *17***: e01370. DOI: https://doi.org/10.1016/j.cscm.2022.e01370.

[4] Y. Yu, X.-Y. Zhao, J.-J. Xu, S.-C. Wang, and T.-Y. Xie, (2022) *"Evaluation of shear capacity of steel fiber reinforced concrete beams without stirrups using artificial intelligence models"* **Materials *15***: 2407. DOI: https://doi.org/10.3390/ma15072407.

[5] Y. Yu, X.-Y. Zhao, J.-J. Xu, S.-C. Wang, and T.-Y. Xie, (2022) *"Evaluation of shear capacity of steel fiber reinforced concrete beams without stirrups using artificial intelligence models"* **Materials *15***: 2407. DOI: https://doi.org/10.3390/ma15072407.

[6] X.-Q. Qu, R. Wang, J.-M. Zhang, and B. He, (2023) *"Influence of soil plug on the seismic response of bucket foundations in liquefiable seabed"* **Journal of Marine Science and Engineering *11***: 598. DOI: https://doi.org/10.3390/jmse11030598.

[7] X. Wu, F. Ding, P. Xiang, Y. Wang, Z. Yu, and C. Liu, (2022) *"Multiaxial damage ratio strength criteria for fiber-reinforced concrete"* **Journal of Engineering Mechanics *148***: 04022029. DOI: https://doi.org/10.1061/(ASCE)EM.1943-7889.0002109.

[8] M. Esmaeili-Falak and R. S. Benemaran, (2024) *"Application of optimization-based regression analysis for evaluation of frost durability of recycled aggregate concrete"* **Structural Concrete *25***: 716–737. DOI: https://doi.org/10.1002/suco.202300566.

[9] S. Kim, M. Usman, C. Park, and A. Hanif, (2021) *"Durability of slag waste incorporated steel fiber-reinforced concrete in marine environment"* **Journal of Building Engineering *33***: 101641. DOI: https://doi.org/10.1016/j.jobe.2020.101641.

[10] C. Frazão, A. Camões, J. Barros, and D. Gonçalves, (2015) *"Durability of steel fiber reinforced self-compacting concrete"* **Construction and Building Materials *80***: 155–166. DOI: https://doi.org/10.1016/j.conbuildmat.2015.01.061.

[11] A. Parvez and S. J. Foster, (2015) *"Fatigue behavior of steel-fiber-reinforced concrete beams"* **Journal of Structural Engineering *141***: 04014117. DOI: https://doi.org/10.1061/(ASCE)ST.1943-541X.0001074.

[12] L. Jin, R. Zhang, G. Dou, and X. Du, (2018) *"Fire resistance of steel fiber reinforced concrete beams after low-velocity impact loading"* **Fire Safety Journal *98***: 24–37. DOI: https://doi.org/10.1016/j.firesaf.2018.04.003.

[13] X. H. Wang, S. Jacobsen, J. Y. He, Z. L. Zhang, S. F. Lee, and H. L. Lein, (2009) *"Application of nanoindentation testing to study of the interfacial transition zone in steel fiber reinforced mortar"* **Cement and Concrete Research *39***: 701–715. DOI: https://doi.org/10.1016/j.cemconres.2009.05.002.

[14] R. Mu, Y. F. Ma, H. Li, X. W. Wang, and P. Zhang, (2015) *"Analysis of the distribution of steel fiber in aligned steel fiber reinforced concrete using digital X-ray CT scanning"* **Journal of Chinese Electron Microscopy Society**: 487–491.

[15] W. Abbass, M. I. Khan, and S. Mourad, (2018) *"Evaluation of mechanical properties of steel fiber reinforced concrete with different strengths of concrete"* **Construction and building materials *168***: 556–569. DOI: https://doi.org/10.1016/j.conbuildmat.2018.02.164.

[16] Y. H. Luo, J. L. Liang, D. S. Yang, B. W. Zhou, B. Hu, and L. Yang, (2018) *"Configuration and operation optimization of electricity-gas-heat energy hub considering reliability"* **Automation of Electric Power Systems *42***: 47–54.

[17] M. H. Jamshidi and M. Arefi, (2024) *"Elastic analysis of functionally graded porous cylinders under uniform internal pressure by using shear deformation theory"* **Mechanics of Advanced Materials and Structures *31***: 11393–11412. DOI: https://doi.org/10.1080/15376494.2024.2304154.

[18] L. Wu, Z. Xiang, H. Jiang, M. Liu, X. Ju, and W. Zhang, (2022) *"A review of durability issues of reinforced concrete structures due to coastal soda residue soil in China"* **Journal of Marine Science and Engineering *10***: 1740. DOI: https://doi.org/10.3390/jmse10111740.

[19] T. Y. Zhu, (2011) *"The mechanical properties of steel fiber-reinforced concrete at low fiber content"* **Zhengzhou: Zhengzhou University**:

[20] M. Açikgenç, M. Ulaş, and K. E. Alyamaç, (2015) *"Using an artificial neural network to predict mix compositions of steel fiber-reinforced concrete"* **Arabian Journal for Science and Engineering *40***: 407–419. DOI: https://doi.org/10.1007/s13369-014-1549-x.

[21] M. Esmaeili-Falak and R. S. Benemaran, (2024) *"Ensemble extreme gradient boosting based models to predict the bearing capacity of micropile group"* **Applied Ocean Research *151***: 104149. DOI: https://doi.org/10.1016/j.apor.2024.104149.

[22] Y. Zhu, L. Huang, Z. Zhang, and B. Bayrami, (2022) *"Estimation of splitting tensile strength of modified recycled aggregate concrete using hybrid algorithms"* **Steel and Composite Structures**: 389–406. DOI: https://doi.org/10.12989/scs.2022.44.3.389.

[23] B. M. Yaychi and M. Esmaeili-Falak, (2024) *"Estimating axial bearing capacity of driven piles using tuned random forest frameworks"* **Geotechnical and Geological Engineering *42***: 7813–7834. DOI: https://doi.org/10.1007/s10706-024-02952-9.

[24] Y. Dawei, Z. Bing, G. Bingbing, G. Xibo, and B. Razzaghzadeh, (2023) *"Predicting the CPT-based pile set-up parameters using HHO-RF and PSO-RF hybrid models"* **Structural Engineering and Mechanics, An Int'l Journal *86***: 673–686. DOI: http://dx.doi.org/10.12989/sem.2023.86.5.673.

[25] R. Liang and B. Bayrami, (2022) *"Estimation of frost durability of recycled aggregate concrete by hybridized Random Forests algorithms"* **Steel and Composite Structures**: 91–107. DOI: https://doi.org/10.12989/scs.2023.49.1.091.

[26] M. Esmaeili-Falak, H. Katebi, M. Vadiati, and J. Adamowski, (2019) *"Predicting triaxial compressive strength and Young's modulus of frozen sand using artificial intelligence methods"* **Journal of Cold Regions Engineering *33***: 04019007. DOI: https://doi.org/10.1061/(ASCE)CR.1943-5495.0000188.

[27] K. Zhang, Y. Zhang, and B. Razzaghzadeh, (2024) *"Application of the optimal fuzzy-based system on bearing capacity of concrete pile"* **Steel and Composite Structures *51***: 25–41. DOI: https://doi.org/10.12989/scs.2024.51.1.025.

[28] M. Açikgenç, M. Ulaş, and K. E. Alyamaç, (2015) *"Using an artificial neural network to predict mix compositions of steel fiber-reinforced concrete"* **Arabian Journal for Science and Engineering *40***: 407–419. DOI: https://doi.org/10.1007/s13369-014-1549-x.

[29] T. F. Awolusi, O. L. Oke, O. O. Akinkurolere, A. O. Sojobi, and O. G. Aluko, (2019) *"Performance comparison of neural network training algorithms in the modeling properties of steel fiber reinforced concrete"* **Heliyon *5***: DOI: https://doi.org/10.1016/j.heliyon.2018.e01115.

[30] O. Karahan, H. Tanyildizi, and C. D. Atis, (2008) *"An artificial neural network approach for prediction of long-term strength properties of steel fiber reinforced concrete containing fly ash"* **Journal of Zhejiang University-SCIENCE A *9***: 1514–1523. DOI: https://doi.org/10.1631/jzus.A0720136.

[31] Y. Şahin and F. Köksal, (2011) *"The influences of matrix and steel fibre tensile strengths on the fracture energy of high-strength concrete"* **Construction and Building Materials *25***: 1801–1806. DOI: https://doi.org/10.1016/j.conbuildmat.2010.11.084.

[32] J. G. Yue, Y. F. Xia, and H. Fang, (2021) *"Experimental study on fracture mechanism and tension damage constitutive relationship of steel fiber reinforced concrete"* **China Civ. Eng. J *54***: 93–106.

[33] I. S. Ibrahim and M. B. C. Bakar, (2011) *"Effects on mechanical properties of industrialised steel fibres addition to normal weight concrete"* **Procedia engineering *14***: 2616–2626. DOI: https://doi.org/10.1016/j.proeng.2011.07.329.

[34] N. Buratti, C. Mazzotti, and M. Savoia, (2011) *"Post-cracking behaviour of steel and macro-synthetic fibre-reinforced concretes"* **Construction and building materials *25***: 2713–2722. DOI: https://doi.org/10.1016/j.conbuildmat.2010.12.022.

[35] B. R. Rajeshwari and M. V. N. Sivakumar, (2020) *"Influence of coarse aggregate properties on specific fracture energy of steel fiber reinforced self compacting concrete"* **Advances in concrete construction**: 173–181. DOI: https://doi.org/10.12989/acc.2020.9.2.173.

[36] Q. Li, Y. Fang, Y. Chen, Q. Wu, G. Lin, and Z. Pang, (2020) *"Experimental study on mechanical properties of concrete with adding steel fiber at early age"* **Concrete *6***: 102–105.

[37] L. L. Niu, S. P. Zhang, and Y. X. Wei, (2019) *"Effect of fiber dosage on the mechanical property of SFRC"* **China Concr. Cem. Prod *3***:

[38] M. Gul, A. Bashir, and J. A. Naqash, (2014) *"Study of modulus of elasticity of steel fiber reinforced concrete"* **Int. J. Eng. Adv. Technol *3***: 304–309.

[39] F. Minelli, A. Conforti, E. Cuenca, and G. Plizzari, (2014) *"Are steel fibres able to mitigate or eliminate size effect in shear?"* **Materials and structures *47***: 459–473. DOI: https://doi.org/10.1617/s11527-013-0072-y.

[40] G. Tiberti, F. Minelli, and G. Plizzari, (2015) *"Cracking behavior in reinforced concrete members with steel fibers: A comprehensive experimental study"* **Cement and concrete research *68***: 24–34. DOI: https://doi.org/10.1016/j.cemconres.2014.10.011.

[41] T. Y. Zhu, (2011) *"The mechanical properties of steel fiber-reinforced concrete at low fiber content"* **Zhengzhou: Zhengzhou University**:

[42] W. Zhao, L. Wang, Z. Zhang, H. Fan, J. Zhang, S. Mirjalili, N. Khodadadi, and Q. Cao, (2024) *"Electric eel foraging optimization: A new bio-inspired optimizer for engineering applications"* **Expert systems with applications *238***: 122200. DOI: https://doi.org/10.1016/j.eswa.2023.122200.

[43] S. Zhao, T. Zhang, S. Ma, and M. Wang, (2023) *"Seahorse optimizer: a novel nature-inspired meta-heuristic for global optimization problems"* **Applied Intelligence *53***: 11833–11860. DOI: https://doi.org/10.1007/s10489-022-03994-3.

[44] G. K. F. Tso and K. K. W. Yau, (2007) *"Predicting electricity energy consumption: A comparison of regression analysis, decision tree and neural networks"* **Energy *32***: 1761–1768. DOI: https://doi.org/10.1016/j.energy.2006.11.010.

[45] S. Araki, M. Shima, and K. Yamamoto, (2018) *"Spatiotemporal land use random forest model for estimating metropolitan NO2 exposure in Japan"* **Science of The Total Environment *634***: 1269–1277. DOI: https://doi.org/10.1016/j.scitotenv.2018.03.324.

[46] H. Hong, H. R. Pourghasemi, and Z. S. Pourtaghi, (2016) *"Landslide susceptibility assessment in Lianhua County (China): a comparison between a random forest data mining technique and bivariate and multivariate statistical models"* **Geomorphology *259***: 105–118. DOI: https://doi.org/10.1016/j.geomorph.2016.02.012.

[47] O. Rahmati, H. R. Pourghasemi, and A. M. Melesse, (2016) *"Application of GIS-based data driven random forest and maximum entropy models for groundwater potential mapping: a case study at Mehran Region, Iran"* **Catena *137***: 360–372. DOI: https://doi.org/10.1016/j.catena.2015.10.010.

[48] J. H. Jeong, J. P. Resop, N. D. Mueller, D. H. Fleisher, K. Yun, E. E. Butler, D. J. Timlin, K.-M. Shim, J. S. Gerber, and V. R. Reddy, (2016) *"Random forests for global and regional crop yield predictions"* **PloS one *11***: e0156571. DOI: https://doi.org/10.1371/journal.pone.0156571.

[49] H. Rao, X. Shi, A. K. Rodrigue, J. Feng, Y. Xia, M. Elhoseny, X. Yuan, and L. Gu, (2019) *"Feature selection based on artificial bee colony and gradient boosting decision tree"* **Applied Soft Computing *74***: 634–642. DOI: https://doi.org/10.1016/j.asoc.2018.10.036.